Combinatorial Methods for Investigations in Polymer Materials Science

J. Carson Meredith, Alamgir Karim, and Eric J. Amis

Abstract

We review recent advances in the development of combinatorial methods for polymer characterization. Applied to materials research, combinatorial methodologies allow efficient testing of structure–property hypotheses (fundamental characterization) as well as accelerated development of new materials (materials discovery). Recent advances in library preparation and high-throughput screening have extended combinatorial methods to a wide variety of phenomena encountered in polymer processing. We first present techniques for preparing continuous-gradient polymer "libraries" with controlled variations in temperature, composition, thickness, and substrate surface energy. These libraries are then used to characterize fundamental properties such as polymer-blend phase behavior, thin-film dewetting, block-copolymer order–disorder transitions, and cell interactions with surfaces of biocompatible polymers.

Keywords: *combinatorial libraries, high-throughput combinatorial methods, microstructure, polymers.*

Introduction

The fundamental characterization of polymers is driven by their applications in structural materials, packaging, microelectronics, coatings, bioengineering, and nanotechnology. Current trends in advanced materials demand finer control of chemistry, morphology, surface patterns, and topography and a focus on multicomponent mixtures, composites, and thin films. These systems are complex due to phase transitions, reactions, transport behavior, and interfacial phenomena that occur during synthesis and processing. In addition, a large number of variables control these complex phenomena, including composition, solvent, temperature, annealing history, pressure, and thickness. Conventional microscopy, spectroscopy, and analytical tools for polymer characterization were designed for detailed characterization over a limited set of variable combinations. These approaches can be used to test hypotheses efficiently if the most relevant variable combinations are known *a priori* or can be predicted from theory. However, the complex phenomena and large variable spaces present in multicomponent, multiphase, and interfacial polymers strain the capabilities of conventional one-sample-for-one-measurement polymer characterization. High-throughput techniques are needed for the efficient synthesis and characterization of complex polymeric systems.

Combinatorial methods present a paradigm for such efficient polymer synthesis and characterization. Combinatorial methods involve a process of (1) experimental design, (2) the creation of sample libraries, (3) high-throughput measurements, and (4) informatics for the efficient modeling of results in the form of structure–property relationships. The key to applying this process to polymers is the availability of techniques to prepare sample "libraries" containing hundreds to thousands of variable combinations each. In addition, high-throughput measurements of the chemical and physical properties of the libraries are needed. The benefits of combinatorial methods include:

- Efficient characterization of novel regimes of thermodynamic and kinetic behavior,
- Rapid testing and identification of structure–property hypotheses,
- Accelerated development of functional materials, and
- Reduced experimental variance due to environmental conditions.

The revival of combinatorial methods within materials science has recently moved from inorganic[1–6] to organic and polymeric materials.[7–18] Unfortunately, the widespread adaptation of combinatorial methods to polymer research had been hindered by a lack of techniques for preparing polymer libraries with systematically varied composition (ϕ), thickness (h), and processing conditions such as temperature (T). In addition, polymer characterization instruments are not typically suitable for high-throughput screening. For this reason, a number of research groups have begun developing library preparation and screening approaches suited for polymer characterization.

Several novel methods have emerged for the preparation of polymer film libraries with continuous gradients in T, ϕ, h, and surface energy (γ). From these libraries, several high-throughput screening methods have been demonstrated for the measurement of polymer-blend phase behavior, block-copolymer segregation, dewetting, and cell–polymer interactions. By focusing this article on characterization, we have omitted discussion of the many successful examples of combinatorial synthesis, experimental design, and informatics for polymers. These encompass a large variety of materials including biodegradable polymers,[7,8,12] support materials for organic synthesis,[11] chemical sensors,[9,13] and dendrimers.[10] The reader is referred to other sources for a review of these topics.[5,19] In order to provide a realistic overview of the types of issues that must be addressed when designing a combinatorial or high-throughput polymer characterization experiment, this article focuses on some of the recent methodology developed at the National Institute of Standards and Technology (NIST).

Preparation of Polymer Coating and Thin-Film Libraries

In contrast to the discrete libraries used in pharmaceutical and catalyst work, the deposition of films with continuous gradients in T, ϕ, h, and γ is often a convenient and elegant method for preparing materials combinatorial libraries.

Thickness-Gradient Libraries

A velocity-gradient knife coater,[16–18] depicted in Figure 1a, was developed to prepare polymer coatings and thin films containing continuous-thickness gradients. A polymer solution is spread under a knife edge onto a substrate at constant acceleration. The velocity gradient results in dried films with controllable thickness gradients. Figure 1c shows h gradients for polystyrene (PS) and poly(4-hydroxystyrene) (PHOS) that cover thicknesses from tens to hundreds of nanometers. By using several h-gradient films with overlapping gradient ranges, thickness-dependent phenomena can be investigated from nanometers to micrometers. Figure 1b shows a photograph of PHOS gradient 3, in which the h gradient produces a continuous change in color and brightness of light reflected from the film–substrate interface.

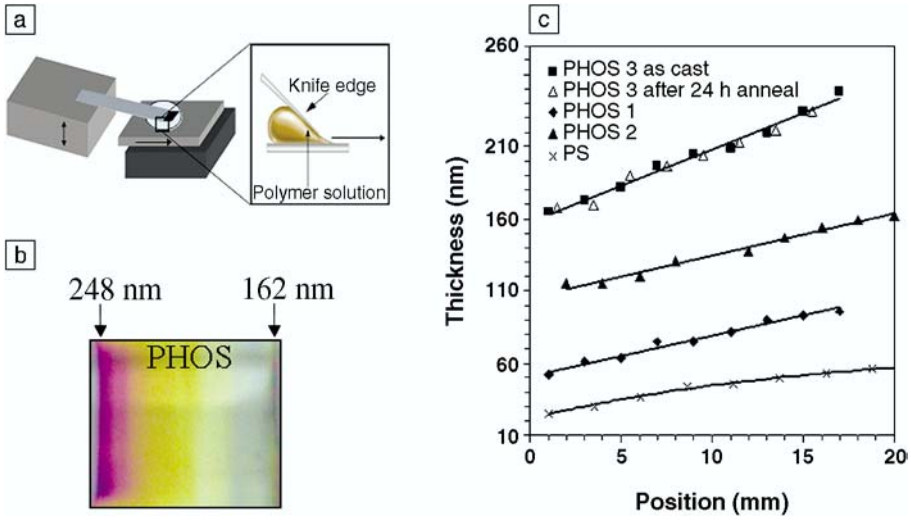

Figure 1. (a) Schematic illustration of the knife-edge coating apparatus. (b) Digital photograph of a thickness-gradient library of poly(4-hydroxystyrene) (PHOS). (c) Thickness gradients in polystyrene (PS) and PHOS films, measured by interferometry. Lines are best fit to the data.

Composition-Gradient Libraries

Three steps are involved in preparing composition-gradient films: gradient mixing (Figure 2a), gradient deposition (Figure 2b), and film spreading (Figure 2c), discussed in detail elsewhere.[16] Two syringe pumps introduce and withdraw polymer solutions A and B to and from a small mixing vial at rates I and W. The infusion of solution A into the pure B solution causes a time-dependent gradient in composition in the vial. A small amount of this solution is continuously extracted with an automated sample syringe. At the end of the sampling process, the sample syringe contains a solution of polymers A and B with a gradient in composition, $\nabla\phi_B$, along the length of the syringe needle. The rates I and W control the slope of the composition gradient, which is linear only if $I = (W + S)/2$ (where S is the flow rate in the sample syringe), and sample time determines the end-point composition. The gradient solution (Figure 2b) is deposited as a thin line on the substrate, and then spread as a film orthogonal to the composition gradient, using a knife-edge coater (Figure 2c). The solvent evaporates, resulting in a film with a continuous linear gradient in composition from polymer A to polymer B. The remaining solvent is removed under vacuum during annealing.

Composition-gradient films of poly(D,L-lactide) (PDLA, Alkermes Medisorb 100DL, M_w = 127,000 g/mol, M_w/M_n = 1.56)* and poly(ε-caprolactone) (PCL, Aldrich, M_w = 114,000 g/mol, M_wM_n = 1.43)† were used to test the ϕ-gradient procedure. Fourier transform infrared (FTIR) spectra were measured with a beam diameter of 500 μm (approximate), significantly larger than the diffusion length of 3 μm (approximate) for the experimental time scale. Films 0.3–1 μm thick were coated on a sapphire substrate, and a translation stage was used to obtain spectra at various positions x (in mm) on the continuous ϕ gradient. Figure 3a shows that PDLA absorbances increase and PCL absorbances decrease as a function of film position (down arrow). Values of the extinction coefficients, $\varepsilon(\nu)$, for pure PDLA and PCL were determined over the C–H stretch regime, 2700–3100 cm^{-1}, based upon $\varepsilon(\nu) = A_i(\nu)/(ch)$, where $A_i(\nu)$ is the measured absorbance for each peak, c is the concentration, and h is the sample thickness. Unknown PDLA/PCL mass fractions were determined to within a standard uncertainty of 4% by assuming that the observed spectra were linear combinations of pure PDLA and PCL spectra. By solving for the linear coefficients required to fit spectra of unknown composition, the mass fraction of PDLA can be determined.[19] Figure 3b shows that a linear gradient is obtained, and the end points and slope agree with those predicted from mass balance.

*Certain equipment and instruments or materials are identified in this article in order to adequately specify the experimental details. Such identification does not imply recommendation by the National Institute of Standards and Technology, nor does it imply the materials are necessarily the best available for the purpose.

†According to ISO 31-8, the term "molecular weight" has been replaced by "relative molecular mass," M_r. The number-average molecular mass is given by M_n. We use the conventionally accepted symbol M_w for weight-average molecular mass.

Temperature-Gradient Libraries

To explore a large T range, the h- or ϕ-gradient films are annealed on a T-gradient heating stage, with the T gradient *orthogonal* to the h or ϕ gradient. This custom aluminum T-gradient stage, described in detail in previous publications,[16,17] uses a heat source and a heat sink to produce a linear gradient ranging between adjustable end-point temperatures. End-point temperatures typically range from 160 ± 0.5°C to 70.0 ± 0.2°C over 40 mm, but are adjustable within the limits of the heater, cooler, and maximum heat flow through the aluminum plate. The error indicates the experimental uncertainty associated with the heating stage. To minimize oxidation and convective heat transfer from the substrate, the stage is sealed with an O-ring, glass plate, and vacuum pump. The two-dimensional T–h parallel library contained about 1800 state points, and the T–ϕ library contained 3900 state points, where a state point is defined by the T, h, and ϕ variation over the area of a 200× optical microscope image: $\Delta T = 0.5$°C, $\Delta h = 3$ nm, and $\Delta\phi = 0.02$. These libraries allow T-, h-, and ϕ-dependent phenomena

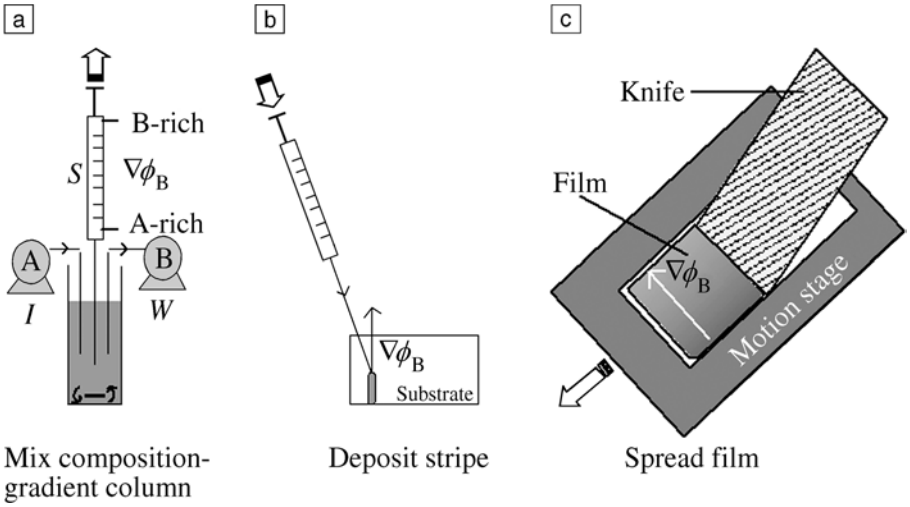

Figure 2. Schematic illustration of the composition-gradient deposition process involving (a) gradient mixing, (b) deposition of stripe, and (c) film spreading (white arrow on the film surface indicates an arbitrary x *axis).* I *is the rate of introduction of a solution of pure polymer A to the mixing vial by means of a syringe pump. An initial fixed volume of pure polymer B solution is pumped into the vial by a syringe pump in the reverse direction of the arrow shown.* W *is the mixed-solution withdrawal rate required to maintain constant volume in the vial,* S *is the solution withdrawal rate in the sampling syringe, and* $\nabla\phi_B$ *is the gradient of polymer B composition in the sampling syringe. See discussion in text for details.*

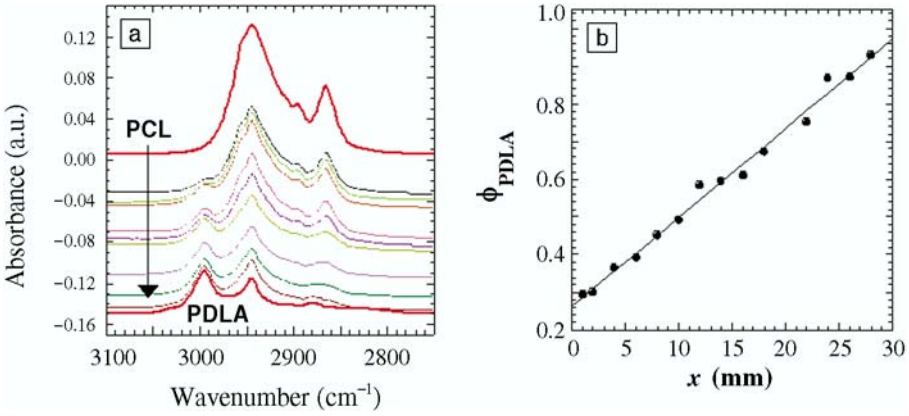

Figure 3. (a) Fourier transform infrared (FTIR) spectra obtained at various spot locations along an arbitrary x *axis (denoted by the white arrow on the film surface in Figure 2c) across a* ϕ*-gradient poly(D,L-lactide)/poly(*ε*-caprolactone) (PDLA/PCL) library, as described in the text. The* x *axis positions were measured in millimeters. PDLA absorptions increase and PCL absorptions decrease as one samples spectra across the film (down arrow). (b) Mass fraction* ϕ_{PDLA} *versus spot location* x *for a PCL/PDLA* ϕ*-gradient library. Standard uncertainty is represented by the symbol size. Line indicates best fit to the data.*

(e.g., dewetting, order–disorder, and phase transitions) to be observed *in situ* or following annealing with relevant microscopic and spectroscopic tools.

Surface-Energy Gradients

For many polymer coating and thin-film systems, there is considerable interest in studying the film stability, dewetting, and phase behavior as a function of surface energy. A gradient-etching procedure has been developed to produce substrate libraries with surface energies varying continuously from hydrophilic to hydrophobic values.[20] The gradient-etching procedure involves the immersion of a passivated Si-H/Si substrate (Polishing Corp. of America) into an 80°C Piranha solution (70%H_2SO_4, 21%H_2O, 9%H_2O_2 by volume) at a *constant immersion rate.* The Piranha bath etches the Si-H surface and grows an oxide layer, SiO_x/SiOH, at a rate dependent on T and the volume fraction of H_2SO_4. A gradient in the conversion to hydrophilic SiO_x/SiOH results because one end of the wafer is exposed to the Piranha solution longer than the other.[20] Another procedure for varying substrate energy uses composition-gradient self-assembled monolayers (SAMs).[21,22] In this procedure, alkanethiolates with different terminal groups (e.g., $–CH_3$ and –COOH) diffuse from *opposite ends* of a polysaccharide matrix deposited on top of a gold substrate. Diffusion produces a SAM with a concentration gradient between the two thiolate species from one end of the substrate to the other, resulting in controllable substrate-energy gradients. These gradient SAM substrates were used to investigate the effect of surface energy on the phase-separation of immiscible polymer blends.[22]

Transport on Gradient Libraries

The introduction of chemical, thickness, and thermal gradients drives nonequilibrium transport processes such as diffusion, flow, and convection that can interfere with phenomena being measured. The time scale and length scale over which gradient library measurements are valid are determined in part by the magnitude of these transport fluxes. In most cases, high-molecular-mass ($M_w > 10{,}000$ g/mol) polymers have relatively low transport coefficients (e.g., diffusivity and flow). Thus, the diffusion and flow length are often orders of magnitude lower than those of the measurements during the relevant time scale, allowing properties to be measured near equilibrium. One can verify that the relatively weak thickness and temperature gradients do not induce appreciable flow in the polymer film over experimental time scales.[16,17] A unidirectional Navier–Stokes model for flow over a flat plate estimates lateral flow at a characteristic velocity of 1 μm/h at $T = 135$°C, in response to gravitational action on the thickness gradient.[23] This small flow is orders of magnitude slower than flows induced by the physical phenomena that these libraries are designed to investigate (e.g., dewetting). To check for flow, thickness-gradient libraries are examined before and after heating, as shown in Figure 1, and the variation in thickness is found to be within the standard uncertainty of ±1.5 nm.

During ϕ-gradient preparation, the gradient in the syringe needle could possibly be homogenized via molecular diffusion. However, the time scale for molecular diffusion is many orders of magnitude larger than the sampling time. Consider gradient solutions of PS and poly(vinyl methyl ether) (PVME) in toluene. For a typical ϕ gradient with $\Delta\phi \approx 0.025$ mm^{-1}, ϕ_{PS} and ϕ_{PVME} at any point are predicted by Fickian diffusion to change by only 0.004%

and 0.001%, respectively, in the 5-min deposition process. Fluid flow in the sample syringe remains laminar, preventing turbulence and convective mixing.[16] In dried ϕ-gradient films, the polymer melt-diffusion coefficients D are typically of the order of 10^{-12} cm^2/s, and diffusion in the cast film can be neglected as long as the length scale resolved in measurements is significantly larger than the diffusion length $\sqrt{Dt}$ that holds for typical microscope resolutions. Measurement of library composition (Figure 3b) and phase behavior (Figure 5b) provides a further proof that diffusion does not significantly alter the ϕ gradients.

Statistical Considerations of Continuous-Gradient Library Measurements

The continuous gradients presented induce an additional variance in observed properties, compared with uniform samples or discrete libraries. For the experiments described here, many of the properties of the polymer continuous libraries are measured from microscope images obtained by optical, fluorescent, or atomic force microscopy (AFM) or from spectroscopy (UV, FTIR). Thus, it is important to understand how uncertainties associated with the gradients and the lateral resolution affect measured properties. Figure 4 demonstrates how a T–ϕ combinatorial library is divided into a grid of virtual measurement sites (e.g., microscope images) of length scale L. The T and ϕ for each measurement site is taken as the average $\langle T\rangle$ and $\langle\phi\rangle$ over the length L. Because of the gradients used, each measurement site has systematic variances $\Delta\phi$ and ΔT that increase as the measurement length scale L increases. Hence, lower measurement resolution (lower L) results in lower $\Delta\phi$ and ΔT. A typical 500 μm × 500 μm image would have reasonable variances of $\Delta\phi = 0.01$ and $\Delta T = 0.3$°C. However, the number of observed features decreases as L decreases, causing an increase in measurement uncertainty and confidence intervals.

A key question to be answered is how to select an optimum measurement scale L that balances the statistical advantage of larger samples (larger L) with the gradient variances $\Delta\phi$ and ΔT. The effects of these contributions on the variance about the mean of any property $\langle p\rangle$ within a measurement site is accounted for using a standard uncertainty propagation,

$$\Delta\langle p\rangle = (\partial\langle p\rangle/\partial N)\,\Delta N + (\partial\langle p\rangle/\partial T)\,\Delta T + (\partial\langle p\rangle/\partial\phi)\,\Delta\phi, \quad (1)$$

where $\langle p\rangle$ is a function of T, ϕ, and the number of observations made in the measurement site, $N \sim L^2$. It is assumed that the number of features (microstructures, cells, etc.) can be counted exactly, so that $\Delta N = 0$. The partial derivatives can be estimated from finite-difference approximations of the measured data, for example,

$$\partial\langle p\rangle/\partial T = [\Sigma p(T_{i+1}, \phi_i) - \Sigma p(T_i, \phi_i)]/[N(T_{i+1} - T_i)]. \quad (2)$$

The values of $\Delta\phi$ and ΔT are $\Delta\phi = m_\phi L$ and $\Delta T = m_T L$, where m_T and m_ϕ are the slopes of the linear gradients, known from the library preparation procedure. Making these substitutions shows that the error propagation for property p scales as

$$\Delta\langle p\rangle \sim (m_T + m_\phi)/L. \quad (3)$$

Constants have been removed in order to reveal only the dependence on gradients and the measurement scale L. Equation 3 demonstrates that uncertainty decreases when L is increased (because more features are counted) and when the gradient magnitude is decreased (reducing ϕ and T variance). The following guidelines should be followed during experimental design and data analysis: (1) L should be as large as possible while still resolving features of interest, and (2) the gradient slopes should be lowered to attain an acceptable uncertainty in the measured property. This analysis considers only uncertainty contributions from the library gradients. Additional sources of uncertainty arise from the measurement steps themselves, but these would also be present for uniform samples and discrete libraries.

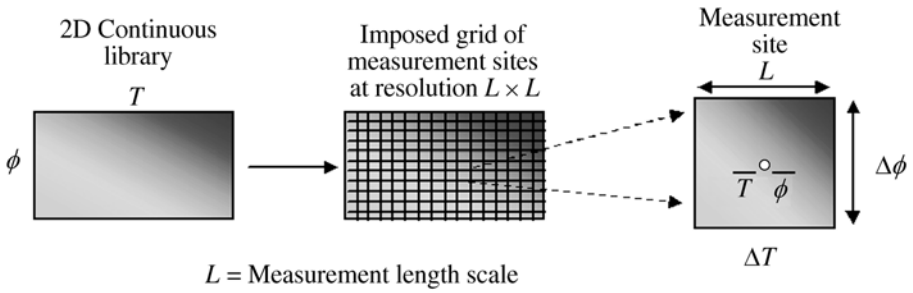

Figure 4. Distribution of discrete measurement sites of resolution L × L *over a continuous-gradient library.* $\overline{T}$ *is the mean temperature and* $\overline{\phi}$ *is the mean composition.*

Fundamental Property Measurement with Combinatorial Polymer Coating and Film Libraries

Thin-Film Dewetting

Wetting and dewetting properties of thin polymer films are of significance in a range of applications in microelectronics, optical communications, and nanotechnology. Figure 5a shows a composite of optical microscope images of a T–h library of PS (Goodyear, $M_w = 1900$ g/mol, $M_w/M_n = 1.19$) on a SiO_x/SiOH substrate.[17,20] The thickness ranges from 33 nm to 85 nm, according to $h = 33.1x^{0.30}$ ($1 < x < 28$) mm and 85°C $< T <$ 135°C. The images, taken 2 h after initiation of dewetting, show wetted and dewetted regimes that are visible as dark and bright regions, respectively, to the unaided eye. Repeated examination of combinatorial T–h libraries at thicknesses ranging from 16 nm to 90 nm indicates three distinct thickness regimes with different hole-nucleation mechanisms. For $h > 55 \pm 4$ nm, discrete circular holes in the film nucleate via heterogeneities (e.g., dust) and grow at a rate dependent on T. Below $h \leq 55 \pm 4$ nm, there is a sharp, temperature-independent transition to a regime where irregular, asymmetrical holes nucleate and grow more slowly than at $h > 55$ nm. In this regime, (33 nm $< h <$ 55 nm), heterogeneous nucleation and capillary-instability nucleation mechanisms compete. The asymmetrical holes present in this regime are surrounded by bicontinuous undulations in the film surface with a characteristic spacing of 7 μm, as indicated by optical microscopy.[17] AFM indicates a roughened surface, with correlated surface undulations indicative of capillary instability or spinodal dewetting. Below $h \approx 33$ nm, another transition in structure and nucleation is apparent. Here, holes are nucleated only by capillary instability and grow more quickly than in the region 33 nm $< h <$ 55 nm. Combinatorial methods thus allow a unique observation of the transition between heterogeneous and capillary-instability nucleation of dewetting, a critical parameter in advanced thin-film materials.[17] This analysis also provided the first observation of a T,h superposition for heterogeneous-nucleated dewetting rates, reflecting variations in the film viscosity with T and h.

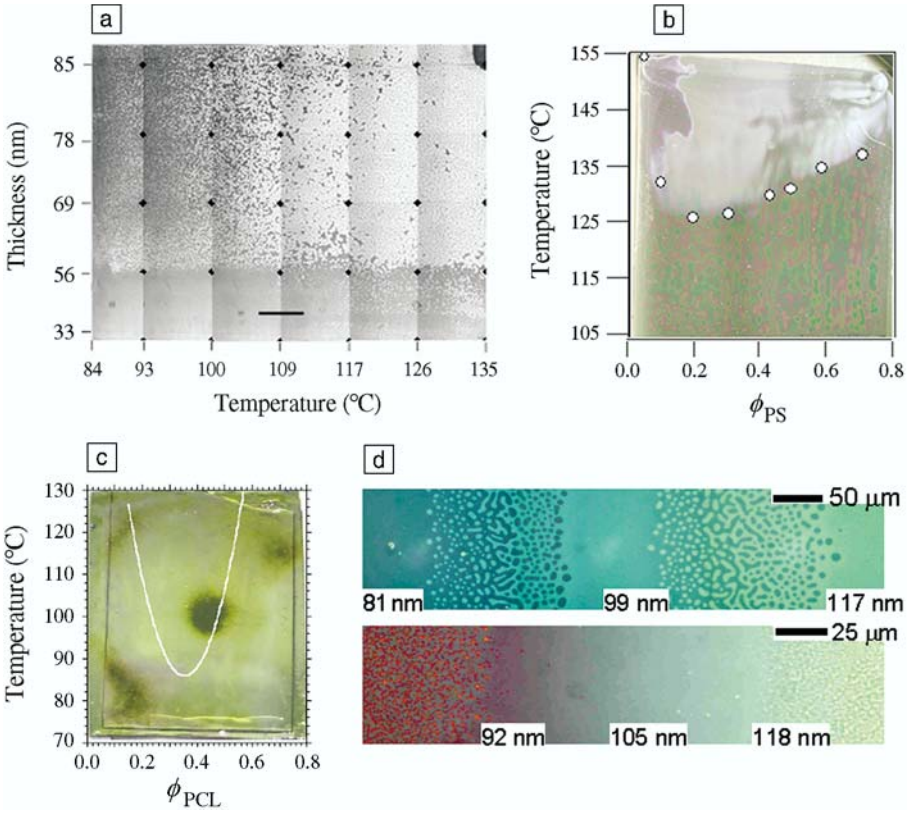

Figure 5. (a) Composite of optical images of a T–h *film dewetting combinatorial library of PS (weight-average molecular mass* M_w *= 1900 g/mol) on silicon,* t *= 2 h, scale bar = (2.0 ± 0.1) mm. (b) Digital optical photographs of a PS and poly(vinyl methyl ether) (PS/PVME)* T–ϕ *library after 16 h of annealing, showing the lower critical solution temperature (LCST) cloud-point curve visible to the unaided eye. White points are conventional light-scattering cloud points measured on separate uniform samples. (c) Alkaline phosphatase (AlP) expression (dark stained areas) for MC3T3-E1 osteoblasts cultured on the surface of a* T–ϕ *library of PDLA and PCL. Cells preferentially express the osteoblast marker AlP only over a small* T, ϕ_{PCL} *region, representing a small distribution of PCL droplet spacings. The white curve is the LCST cloud-point curve for PDLA and PCL. (d) Optical micrograph of a* M_w *= 26,000 g/mol (top) and* M_w *= 104,000 g/mol (bottom) PS-*b*-poly(methyl methacrylate) gradient film, showing the addition of lamellae to the surface with increasing thickness. Standard uncertainty in thickness is ±3 nm.*

Phase Behavior

The phase-separation and related microstructure of polymer blends is of critical importance in many engineered plastics, but traditional determination of phase behavior for new blends and blends with additives remains a tedious task. Figure 5b presents a photograph of a temperature-composition library of a PS/PVME blend (discussed earlier in the transport properties section) after 16 h of annealing. The lower critical solution temperature (LCST) cloud-point curve can be seen with the unaided eye as a diffuse boundary separating one-phase and two-phase regions. Cloud points measured with conventional light scattering on bulk samples (white points) agree well with the cloud-point curve observed on the library.[16] The diffuse nature of the cloud-point curve reflects the natural dependence of the microstructure evolution rate on temperature and composition. We expect only a negligible effect on the observed LCST, based on bulk diffusion coefficients and the annealing time of 2 h, which means each pixel in Figure 5b covers about 30 μm, over 100 times the diffusion length. The combinatorial technique employing T–ϕ polymer-blend libraries allows for rapid and efficient characterization of polymer-blend phase behavior (cloud points) in orders of magnitude less time than with conventional light-scattering techniques.

Cell Culturing

Phase-separation offers a potential method for the preparation of porous three-dimensional scaffolds for tissue engineering or drug delivery. The combinatorial approach has been extended to allow investigation of the adhesion and function of biological cells as a function of surface-patterned microstructure. Phase-separated libraries of biodegradable polymers can be cultured with cells, exposing the cells to a wide variety of surface features in a single experiment. These library cultures are amenable to staining, microscopy, and spectroscopy to determine cell response to surface features. In Figure 5c, T–ϕ_{PCL} combinatorial libraries of biodegradable PDLA and PCL exhibit LCST phase behavior at $T > 86$°C. After 2 h annealing, the feature size of PCL-rich domains varies from about 100 nm to over 100 μm as a function of annealing temperature and ϕ_{PCL}, along with a concomitant variation in surface roughness, determined from AFM, of 2–400 nm.[24] Cell-culturing studies were performed to ascertain the effect of phase-separated microstructure on the function of MC3T3-E1 osteoblasts (bone cells). After culturing for five days, cultures were rinsed with phosphate-buffered saline and fixed in a 70 vol% ethanol/30 vol% water solution for 30 min. Figure 5c presents a digital photograph of a library culture after staining for the osteoblast marker alkaline phosphatase (AlP).[25] The darkest stained circular region near the center of the library indicates enhanced AlP expression, relative to the other T, ϕ_{PCL} regions and a tissue-culture polystyrene (TCPS) control. This combinatorial library indicates that AlP expression is a strong function of the microstructures present on the phase-separated PDLA/PCL-blend surface. The white curve in Figure 5c is the LCST cloud-point curve for this blend.[26] The region of enhanced AlP corresponds to a processing temperature of 96–110°C and $0.4 < \phi_{PCL} < 0.55$, only 5% of the total library surface. In contrast, MC3T3-E1 cultured concurrently on uniform TCPS shows uniform AlP expression. The enhanced AlP regime could be missed entirely or misinterpreted as aberrant if the T and ϕ range were screened with a small number of individual samples, as is the conventional practice. Such an approach allows the identification of biomaterial surfaces that elicit desired biological responses prior to a time-consuming characterization regime. As a result, structure–property hypotheses could then be explored in detail using conventional techniques for the most promising materials.

Block-Copolymer Segregation and Surface Morphology

The morphology of symmetric diblock-copolymer thin films has been studied extensively with traditional techniques.[27–29] These materials hold potential as templates for nanostructural patterning of surfaces. Because of the thickness dependence in these systems, the fundamental investiga-

tion of block-copolymer segregation is ideal for the use of *h*-gradient combinatorial methods.[18,30] Films of symmetric polystyrene-*b*-poly(methyl methacrylate) (PS-*b*-PMMA) with *h* gradients were produced using the knife-edge flow-coating technique. The libraries were annealed at 170°C for 30 h to allow lamellar organization. Figure 5d presents optical micrographs showing morphological changes associated with the addition of two lamellae to the surface of the film as *h* increases. This is in agreement with previous (noncombinatorial) work showing that lamellae with thicknesses equal to the equilibrium bulk lamellar thickness L_0 form parallel to the substrate.[27–29] The lamellae form smooth films when the total film thickness *h* is equal to a half-integral multiple *m* of L_0, for example, $h \approx (m + 1/2)L_0$, when PMMA prefers the substrate and PS prefers the air interface. When *h* deviates from these values, holes or islands of height L_0 are found to form on the film surface in order to reduce the system energy. Labels in Figure 5d denote approximate *h* values corresponding to $h \approx (m + 1/2)L_0$ for $m = 4$, 5, and 6. The morphology evolves from a smooth film to circular islands to a bicontinuous hole/island region to circular holes and back to a smooth film (from left to right in the micrograph) and repeats twice. This result represents the first observation of stable bicontinuous morphologies in segregating block-copolymer thin films.[18,30] Another novel observation enabled by combinatorial methods is the wide thickness range over which the smooth film regions persist. Notably, the smooth regions of the film form a significant fraction of the morphology, corresponding to a thickness range Δh deviating significantly from a half-integral multiple of L_0. The value of Δh is $\approx 0.28L_0$ and is invariant within standard uncertainty for all M_w and *h* investigated. This effect is interpreted to arise from a brushlike stretching and compression of block-copolymer chains in the outer lamella as the chain density varies with *h*. This work on block-copolymer morphology provides an excellent example of how the combinatorial technique allows the exploration of new understanding in traditional topics of materials science study.

Organic Light-Emitting Diodes

As the final example, we discuss here two characterization studies of the optimization of organic light-emitting diodes (OLEDs). Schmitz and co-workers[14,31,32] used a masked deposition technique to produce *thickness gradients* in both the organic hole-transport layers and the inorganic electron-transport and emitting layers. OLEDs with single-gradient and orthogonal two-dimensional gradient structures were produced in order to evaluate the effects of the various layer thicknesses on the device efficiency. An optimal thickness for both the hole- and electron-transporting layers was reported. Likewise Gross et al. have reported the use of combinatorial methods to investigate the performance of doped (oxidized) π-conjugated polymers in OLEDs.[15] In these devices, the polymers serve as hole-transport layers, but an energy barrier for hole injection exists between the polymeric material and the inorganic anode. By varying the oxidation level of the polymer, this energy barrier can be reduced to lower the device working voltage. The effect of oxidation was studied by electrochemically treating the polymer to create a continuous gradient in the oxidation level of the polymer. A gradient in thickness was created orthogonal to the gradient in oxidation to explore variations of both properties simultaneously. For this reason, this study represents a cross between both combinatorial synthesis (oxidation steps) and process characterization (thickness gradient deposition). The gradient libraries were characterized by monitoring the efficiency and onset voltage of OLEDs fabricated on the gradients.

Conclusions

In this brief review, we have presented recent advances in which combinatorial methodologies have been used to efficiently measure chemical, physical, and biological properties of polymers over large regimes of variable space. These new approaches allow for both materials discovery and the development of new models and structure–processing–property relationships. We presented four techniques for preparing continuous-gradient polymer libraries with controlled variations in temperature, composition, thickness, and substrate surface energy. These libraries, coupled with automated spectroscopy and microscopy, facilitate characterization of polymer-blend phase behavior, thin-film dewetting, block-copolymer order–disorder transitions, cell response to polymer surface features, and other phenomena.

Acknowledgment

J.C. Meredith acknowledges the National Research Council for a NIST postdoctoral associateship. Funding was provided by the NIST Advanced Technology Program and the ACS Petroleum Research Fund.

References

1. E. Reddington, A. Sapienza, B. Gurau, R. Viswanathan, S. Sarangapani, E. Smotkin, and T. Mallouk, *Science* **280** (1998) p. 1735.
2. J. Wang, Y. Yoo, C. Gao, I. Takeuchi, X.-D. Sun, H. Chang, X.-D. Xiang, and P.G. Schultz, *Science* **279** (1998) p. 1712.
3. X.-D. Sun and X.-D. Xiang, *Appl. Phys. Lett.* **72** (1998) p. 525.
4. E. Danielson, M. Devenney, D.M. Giaquinta, J.H. Golden, R.C. Haushalter, E.W. McFarland, D.M. Poojary, C.M. Reaves, W.H. Weinberg, and X.D. Wu, *Science* **279** (1998) p. 837.
5. B. Jandeleit, D.J. Schaefer, T.S. Powers, H.W. Turner, and W.H. Weinberg, *Angew. Chem., Int. Ed. Engl.* **38** (1999) p. 2494.
6. J. Klein, C.W. Lehmann, H.-W. Schmidt, and W.F. Maier, *Angew. Chem., Int. Ed. Engl.* **37** (1998) p. 3369.
7. S. Brocchini, K. James, V. Tangpasuthadol, and J. Kohn, *J. Am. Chem. Soc.* **119** (1997) p. 4553.
8. S. Brocchini, K. James, V. Tangpasuthadol, and J. Kohn, *J. Biomed. Mater. Res.* **42** (1998) p. 66.
9. T.A. Dickinson, D.R. Walt, J. White, and J.S. Kauer, *Anal. Chem.* **69** (1997) p. 3413.
10. G.R. Newkome, C.D. Weis, C.N. Moorefield, G.R. Baker, B.J. Childs, and J. Epperson, *Angew. Chem., Int. Ed. Engl.* **37** (1998) p. 307.
11. D.J. Gravert, A. Datta, P. Wentworth, and K.D. Janda, *J. Am. Chem. Soc.* **120** (1998) p. 9481.
12. C.H. Reynolds, *J. Comb. Chem.* **1** (1999) p. 297.
13. T. Takeuchi, D. Fukuma, and J. Matsui, *Anal. Chem.* **71** (1999) p. 285.
14. C. Schmitz, P. Posch, M. Thelakkat, and H.W. Schmidt, *Macromol. Symp.* **154** (2000) p. 209.
15. M. Gross, D.C. Muller, H.G. Nothofer, U. Sherf, D. Neher, C. Brauchle, and K. Meerholz, *Nature* **405** (2000) p. 661.
16. J.C. Meredith, A. Karim, and E.J. Amis, *Macromolecules* **33** (2000) p. 5760.
17. J.C. Meredith, A.P. Smith, A. Karim, and E.J. Amis, *Macromolecules* **33** (2000) p. 9747.
18. A.P. Smith, J. Douglas, J.C. Meredith, A. Karim, and E.J. Amis, *Phys. Rev. Lett.* **87** (2001) p. 15503.
19. J.C. Meredith, A. Karim, and E.J. Amis, in *ACS Symposium Series: Combinatorial Approaches to Materials Development,* edited by R. Malhotra (American Chemical Society, Washington, DC, 2001).
20. K. Ashley, J.C. Meredith, A. Karim, and D. Raghavan, *Polym. Commun.* (2000) in press.
21. B. Liedberg and P. Tengvall, *Langmuir* **11** (1995) p. 3821.
22. J. Genzer and E.J. Kramer, *Europhys. Lett.* **44** (1998) p. 180.
23. L.G. Leal, *Laminar Flow and Convective Transport Processes* (Butterworth-Heinemann, Boston, 1992).
24. J.C. Meredith, A. Garcia, A. Tona, A. Karim, and E.J. Amis (unpublished manuscript).
25. O.A. Bessey, O.H. Lowry, and M.J. Brock, *J. Biol. Chem.* **164** (1946) p. 321.
26. J.C. Meredith and E.J. Amis, *Macromol. Chem. Phys.* **200** (2000) p. 733.
27. H. Hasegawa and T. Hashimoto, *Macromolecules* **18** (1985) p. 589.
28. T.P. Russell, G. Coulon, V.R. Deline, and D.C. Miller, *Macromolecules* **22** (1989) p. 4600.
29. M.J. Fasolka and A.M. Mayes, *Annu. Rev. Mater. Res.* **31** (2001) p. 323.
30. A.P. Smith, J. Douglas, J.C. Meredith, A. Karim, and E.J. Amis, *J. Polym. Sci., Part B: Polym. Phys.* **39** (2001) p. 2141.
31. C. Schmitz, M. Thelakkat, and H.W. Schmidt, *Adv. Mater.* **11** (1999) p. 821.
32. C. Schmitz, P. Posch, M. Thelakkat, and H.W. Schmidt, *Phys. Chem. Chem. Phys.* **1** (1999) p. 1777. □